JOURNAL OF MATERIALS SCIENCE 31 (1996) 1663–1668

Determination of microstructural anisotropy in Sb–InSb eutectic by electrical resistivity measurement

MYUNG-JIN SUK, GIL-HEYUN CHOI*, IN-HYUNG MOON
Department of Materials Engineering, Hanyang University Seoul 133–791, Korea

The longitudinal, $\rho\parallel$, and transverse, $\rho\perp$, resistivities have been measured in Sb–InSb eutectic alloys unidirectionally solidified over a range of growth rates, 1.2×10^{-4} to 1.2×10^{-1} cm s^{-1}. The measured resistivities differ from the theoretical values estimated on the basis of macroscopic geometrical approximation for the spatial arrangement of Sb rods within the InSb matrix. The difference between the two is explained in terms of the contribution of the interface phase, as well as the loss of microstructural anisotropy. In the present work the interface between the Sb rod and the InSb matrix was regarded as a definite phase constituting an *in situ* eutectic composite. The presence of this interfacial phase was assumed to result in an increase of $\rho\perp$. The degree of microstructural anisotropy, δ, is defined from the geometrical relation determined by the $\rho\parallel$ value, allowing quantitative description of microstructural anisotropy. As expected, δ gradually decreases with increasing growth rate. Some of the quickly grown specimens have revealed radial directionality in their microstructure, which is reflected by the relative size of $\rho\parallel$ and $\rho\perp$ values.

1. Introduction

The fact that electrical resistivity may be one of the most microstructure sensitive properties makes it possible to depict the microstructural features of materials in terms of their electrical resistivities. Considerable interest in this connection has been drawn to the field of heterogeneous materials, including eutectic alloys, as well as other artificial composites [1–4].

So far a number of models have been developed for calculating theoretically the electrical resistivities of the composite as a function of the structural parameters, such as the volume fraction of the constituent phases and their geometrical arrangements [5–9]. Some of these are deduced on the basis of mathematical analogy between the general transport phenomena in composite structure, e.g. electrical conduction, thermal conduction, dielectric behaviour, etc. [5]. Since Liebmann and Miller's work on Sb–InSb eutectic composites [8], few researches, other than its modified version by Digges and Tauber [9], have been conducted for theoretically describing the electrical resistivity of the eutectic composites. Their approaches assume that simple electrical analogues of eutectic structure have an advantage in their simplicity, which allows easier understanding of the macroscopic geometrical arrangement of the constituent phases.

It is well known that eutectic alloys show a variety of microstructures with growth parameters. The variation of microstructure includes alignment of the constituent phases along the growth direction (microstructural anisotropy), as well as their individual morphologies.

The present experimental results have already been qualitatively interpreted in a previous report [10]. The present paper partly revises the previous analysis and describes more quantitatively the microstructural variation of the unidirectionally solidified Sb–InSb eutectic composite in the context of microstructural anisotropy. The electrical resistivity of the alloys was interpreted by assuming an appropriate geometrical arrangement of the Sb rods in a similar manner to the approach by Liebmann and Miller [8] and Digges and Tauber [9]. The Sb–InSb alloy system was adopted for the present work because it shows ideal eutectic behaviour with complete immiscibility in each constituent phase, providing simplicity in determining the resistivities of the constituent phases.

2. Experimental procedure

Sb–InSb alloys near eutectic composition were prepared from 99.999% pure Sb and In, and encapsulated in an evacuated (13.33 Pa) quartz tube (6 mm internal diameter). The alloys were then melted and unidirectionally solidified in a Bridgman type vertical furnace with traction rates ranging from 1.2×10^{-4} to 1.2×10^{-1} cm s^{-1}. The traction rate was assumed to

* *Present address*: Research Group 2, Kihung R&D Center, Samsung Electronics, P.O. Box 107, Suwon 440–600, Korea.

0022–2461

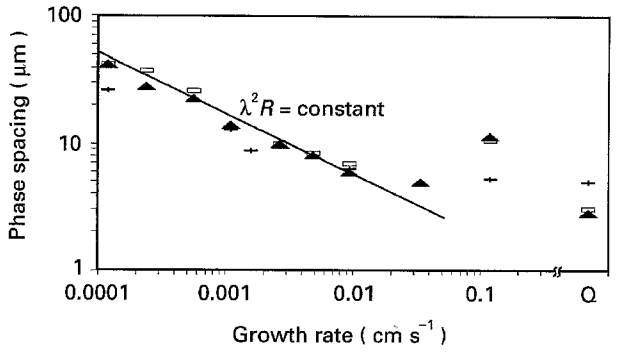

Figure 1 Variation of interphase spacing with growth rate. (▲) Sb–26 wt % In, (+) Sb–29 wt % In, (□) Sb–33 wt % In.

be equal to the growth rate (throughout this paper growth rate simply means traction rate of the specimen), but as implied from Fig. 1 this relation is no longer maintained at fast traction rates ($> 3 \times 10^{-2}$ cm s^{-1}). Some specimens were water quenched and are indicated as "Q" in the figures and table. More detailed descriptions of the specimen preparation and solidifying conditions are given elsewhere [11].

The samples used for electrical resistivity measurements were cut from the middle part of the solidified specimen, where steady state growth is confirmed to be achieved, and were ground to the form of a $4 \times 4 \times 4$ mm cube. Three samples were obtained from each specimen with a given solidifying condition. The resistivity was measured at room temperature using the four probe method by means of a nanovoltmeter (Keithley 181) and current source (Keithley 228A). Measurement of resistivity was made both in a longitudinal and transverse direction, and at least 15 readings were taken for each sample. The length of the sample may be thought of as too short to ensure accurate measurement of electrical resistivity, because the voltage terminals may be positioned so close to the current terminals that a non-uniform equipotential line of the electric field may develop [12]. In order to overcome this problem an appropriate sample holder was used; in this sample holder two indium bars (1 cm long) which were in contact with both sides of the sample were strongly pushed in opposite directions by two movable current terminals, so that a tight areal contact could be maintained between the indium bars and the sample. The resulting effect is to lengthen the sample size by the length of the indium bars. The resistivities of same sized pure (99.999%) materials (Sb, Sn and Bi) measured in this holder gave good agreement with those in [13]. Interphase spacing was measured on transverse sections by counting the number of line intercepts with the aid of an image analyser (Leco 2001).

3. Results

Fig. 2 shows typical transverse and longitudinal microstructures of Sb–InSb eutectics obtained at different growth rates. Regular arrays of triangular Sb rods readily develop at lower growth rates, indicating well defined microstructural anisotropy of the *in situ* composite. At higher growth rates, on the other hand, the directionality of the microstructure decreases considerably, and the angular morphology of the Sb fibres is changed to a round shape. Colony structure, which is characterized by the formation of a eutectic cell, can be also found in Fig. 2c, d.

The variation of electrical resistivity as a function of growth rate is given in Fig. 3. With increasing growth rate, the longitudinal resistivity, $\rho\|$, increases steeply, whereas the transverse resistivity, $\rho\perp$, shows a gradual decrease. The only exception to this $\rho\perp$ trend is made for the specimen with 26 wt % In grown at 1.2×10^{-4} cm s^{-1}, and will be briefly discussed in the next section.

Interphase spacing, λ, of Sb–InSb eutectics of various compositions is plotted against growth rate, R, in Fig. 1. In this logarithmic plot a linear relation between the interphase spacing and the growth rate is preserved up to a growth rate of about 10^{-2} cm s^{-1}, with the slope of the line being $-1/2$. This relation has been generally accepted as one of the major characteristics of eutectic growth. Deviation from the linear relation at higher growth rate is attributed to unidirectional–equiaxed transition of the solidification mode. At higher specimen traction rates, heat transfer within the specimen starts to change from unidirectional to three-dimensional, with the result that the actual growth rate is no longer equal to the traction rate.

4. Discussion

4.1. Microstructural anisotropy

Each Sb rod in Fig. 2a, b can be consolidated into a rectangular parallelepiped configuration of Sb block in a unit cube, as shown in Fig. 4. If the Sb rods are completely aligned without introducing any type of faults in their longitudinal array, y equals 1. This condition, however, is scarcely met, and some inherent faults in many forms, e.g. broken rods, exist even in the carefully controlled growth process of unidirectional solidification, as exemplified in Fig. 2b; in this case y is less than 1. The crosshatched area in Fig. 4 denotes the consolidated configuration of the interfaces between the elongated Sb rod and the InSb matrix. In the present paper the interface is regarded as a constituent phase of this *in situ* composite, which is expected to have much higher resistivity than both Sb and InSb due to the disturbances in its atomic arrangement. The presence of this interface phase has been neglected in calculating the theoretical resistivities of the eutectic composites [8, 9], but it should be taken into account for more rigorous evaluation. In this configuration the interfaces in front of the Sb block in the longitudinal direction are disregarded because their volume fraction is extremely small, compared to those located at the sides of the Sb block.

The resistivities in transverse, $\rho\perp$, and longitudinal, $\rho\|$, directions of such a composite can be derived in terms of simple electrical resistor analogues, as already used elsewhere [8, 9]. If it is assumed that the interface phase has a negligible effect on the electrical

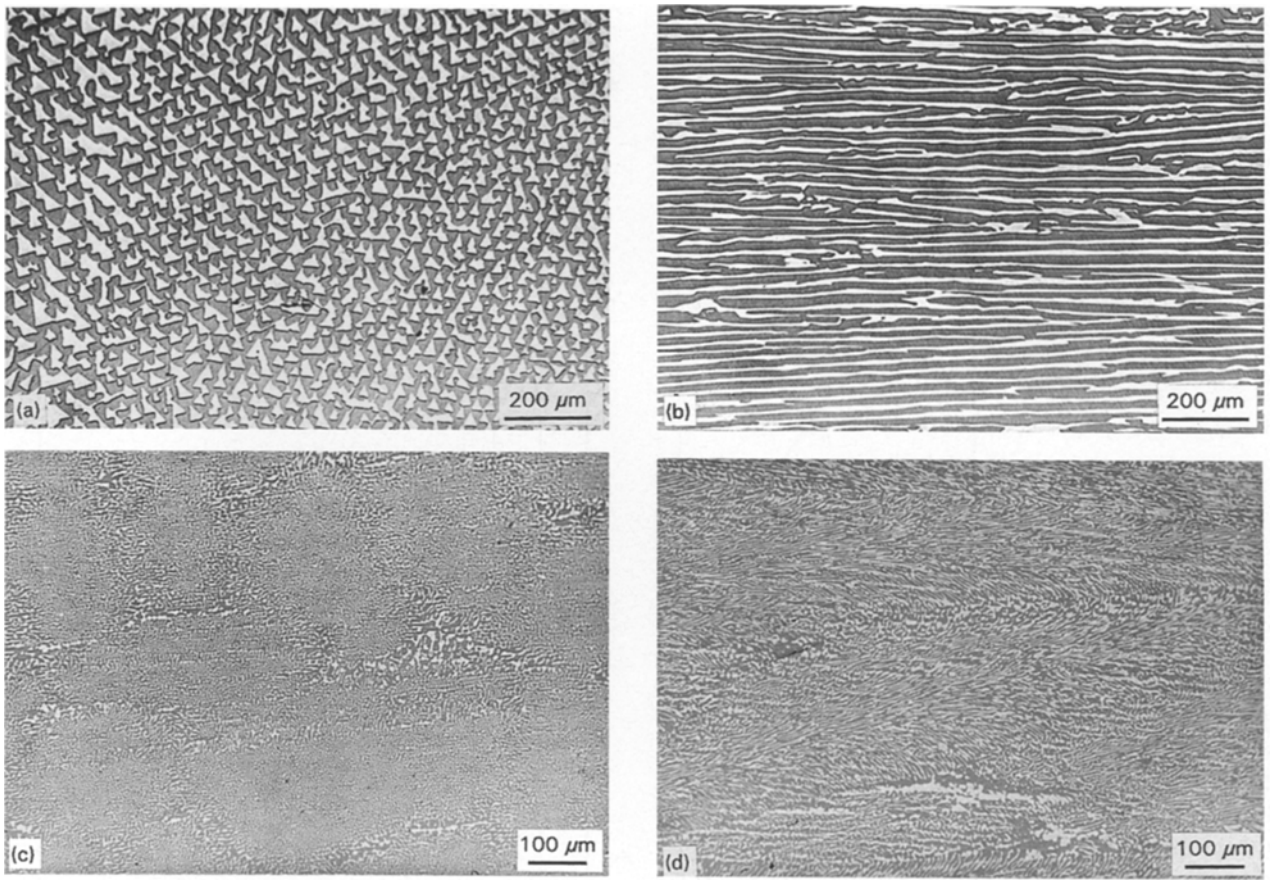

Figure 2 Typical microstructure of Sb–InSb eutectics (29 wt % In). (a) transverse section, $R = 1.2 \times 10^{-4}$ cm s^{-1}, (b) longitudinal section, $R = 1.2 \times 10^{-4}$ cm s^{-1}, (c) transverse section, $R = 9.4 \times 10^{-3}$ cm s^{-1}, and (d) longitudinal section, $R = 9.4 \times 10^{-3}$ cm s^{-1}.

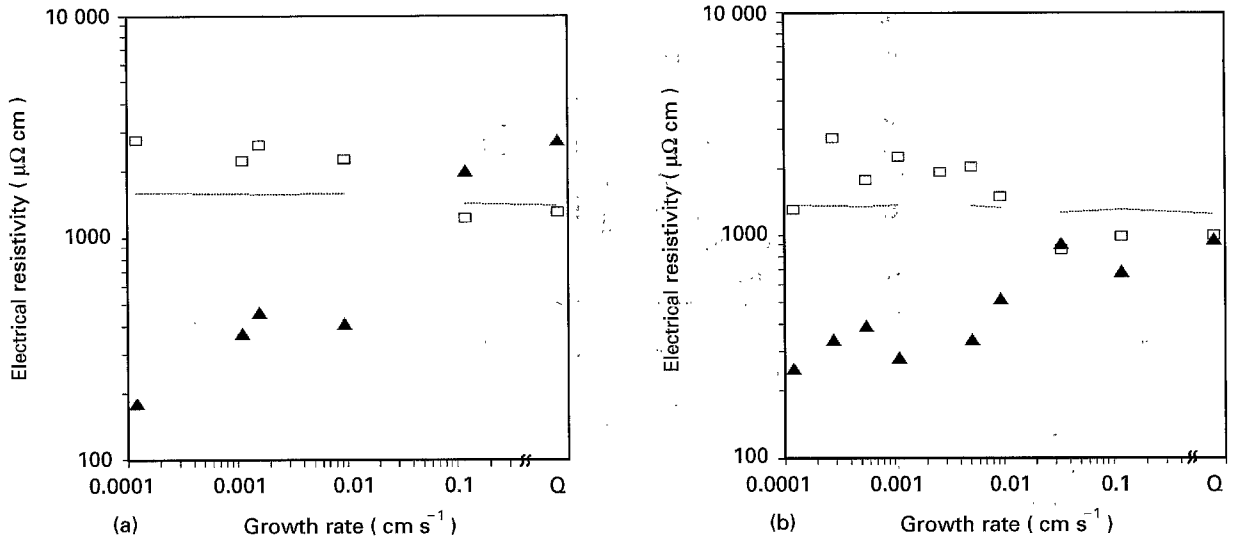

Figure 3 Dependence of electrical resistivities on growth rate: (a) (29 wt % In), and (b) 26 wt % In (□ ρ⊥), (▲ ρ∥).

resistivities, then

$$\frac{1}{\rho\parallel} = \frac{y - V_{Sb}}{y\rho_{InSb}} + \frac{V_{Sb}}{y[y\rho_{Sb} + (1-y)\rho_{InSb}]} \quad (1)$$

$$\frac{1}{\rho\perp} = \frac{x - V_{Sb}}{x\rho_{InSb}} + \frac{V_{Sb}}{x[x\rho_{Sb} + (1-x)\rho_{InSb}]} \quad (2)$$

where V_{Sb} is the volume fraction of Sb, and ρ_{Sb} and ρ_{InSb} are resistivities of Sb and InSb, respectively. If an ideal alignment of the Sb rods is assumed, i.e. $y = 1$, Equations 1 and 2 give ρ⊥ and ρ∥ as 1380 and 93 μΩ cm for 26 wt % In and 1590 and 108 μΩ cm for 29 wt % In, respectively. In this calculation the resistivity of Sb is taken as 41 μΩ cm [13], and that of InSb is 3050 ± 50 μΩ cm, which was measured in the pure InSb specimen prepared in the same way as the other alloy specimens.

The slowly grown specimens are expected to show relatively good alignment of Sb rods, though not completely ideal, allowing for less faults to be formed. However, the measured electrical resistivities in

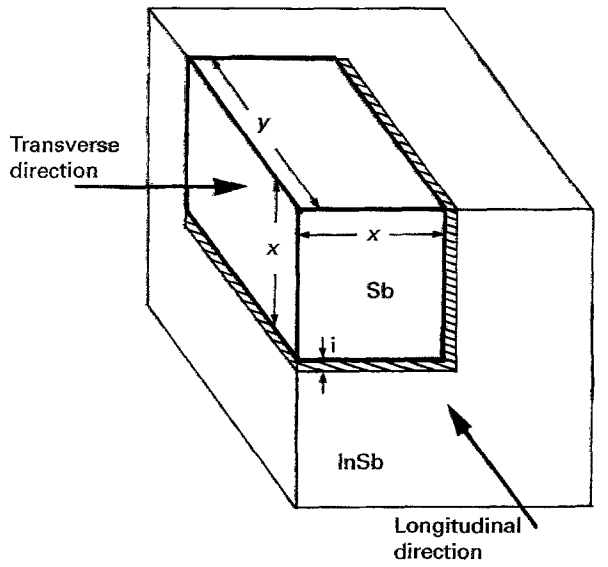

Figure 4 Schematic representation showing the consolidated configuration of Sb and interface phase within InSb matrix.

Fig. 3 are quite different from the ideally calculated ones. This mismatch can be explained by considering the faults which exist practically to a considerable degree in the longitudinal arrangement of the Sb rods (in the case of $\rho\parallel$), and incorporating the effect of the interface phase which was neglected in the above calculation (in the case of $\rho\perp$). Since $\rho\parallel$ will be hardly influenced by the presence of a lateral interface phase lying parallel to the Sb block, the values of y and x can be obtained from the experimentally measured $\rho\parallel$ using Equation 1; the y value being taken directly from the equation, and the x value from the relation $x^2y = V_{Sb}$. The y and x values are listed in Table I. $\rho\perp$ is theoretically calculated by putting these y and x values into Equation 2, and is indicated as a dashed line in Fig. 3. However, a somewhat larger discrepancy lies between the calculated and the measured $\rho\perp$ values, the latter being higher than the former (up to growth rates of about 10^{-2} cm s^{-1}). The increase in $\rho\perp$ is attributed to the interface phase, because it partly makes a serial arrangement together with Sb and InSb, exerting a serious effect on the transverse resistivity value.

In the fast grown specimens the microstructure does not show directionality parallel to specimen movement, but rather equiaxed nature or even radial directionality. The transition of the directionality is reflected by the higher value of $\rho\parallel$ and $\rho\perp$ in Fig. 3. In this case the transverse and longitudinal directions in Fig. 4 should change with each other, and the corresponding value of y and x are calculated by putting the experimentally measured $\rho\perp$ value instead of the $\rho\parallel$ into Equation 1.

Since the y and x values specify the spatial arrangements of the constituent phases with regard to the longitudinal and the transverse directions, their relative size can be a measure of the degree to which the microstructural anisotropy is attained. The degree of anisotropy, δ, can be defined as follows

$$1 - \delta = \frac{V_{Sb}^{-1/2} - k}{V_{Sb}^{-1/2} - 1} \quad (3)$$

TABLE I Summary of the data concerned with the calculation of electrical resistivities

		Growth rate (cm s^{-1})									
		1.2×10^{-4}	2.8×10^{-4}	5.6×10^{-4}	1.1×10^{-3}	1.6×10^{-3}	5.2×10^{-3}	9.4×10^{-3}	3.4×10^{-2}	1.2×10^{-1}	Q
Sb–29 wt % In	Measured $\rho\parallel$, $\mu\Omega$ cm	180			370	460		420		1220[a]	1290[a]
	y	0.990			0.963	0.948		0.956		0.767	0.742
	x	0.611			0.620	0.625		0.622		0.695	0.706
	k	1.620			1.552	1.517		1.537		1.104	1.052
	δ	0.963			0.858	0.803		0.834		0.162	0.080
	Calculated $\rho\perp$, $\mu\Omega$ cm	1589.0			1572.2	1562.9		1568.2		1412.0	1385.0
	Sb rod diameter, μm	16.00			7.85	5.35		3.83		3.16	2.98
	Measured $\rho\perp$, $\mu\Omega$ cm	2770.0			2120.0	2620.0		2250.0		1980.0	2720.0
	ρ^i, $\mu\Omega$ cm	2.6×10^7			6.1×10^6	7.5×10^6		3.2×10^6		1.8×10^6	4.7×10^6
Sb–26 wt % In	Measured $\rho\parallel$, $\mu\Omega$ cm	250	340	390	280		340	520	850[a]	680	940
	y	0.975	0.960	0.951	0.970		0.960	0.925	0.847	0.890	0.822
	x	0.664	0.669	0.673	0.666		0.669	0.682	0.712	0.695	0.723
	k	1.469	1.434	1.413	1.457		1.434	1.357	1.190	1.281	1.137
	δ	0.893	0.826	0.787	0.871		0.826	0.680	0.361	0.535	0.260
	Calculated $\rho\perp$, $\mu\Omega$ cm	1367.7	1356.1	1349.1	1364.0		1356.1	1328.7	1256.2	1298.1	1229.0
	Sb rod diameter, μm	27.48	18.43	14.75	9.18		5.31	3.87	3.21	7.41	1.84
	Measured $\rho\perp$, $\mu\Omega$ cm	1300	2740	1770	2250		2020	1490	900	980	990
	ρ^i, $\mu\Omega$ cm		3.1×10^7	6.4×10^6	9.0×10^6		3.8×10^6	6.0×10^5			

[a] In these specimens radial directionality was obtained, and thus $\rho\parallel$ and $\rho\perp$ were interchanged with each other.

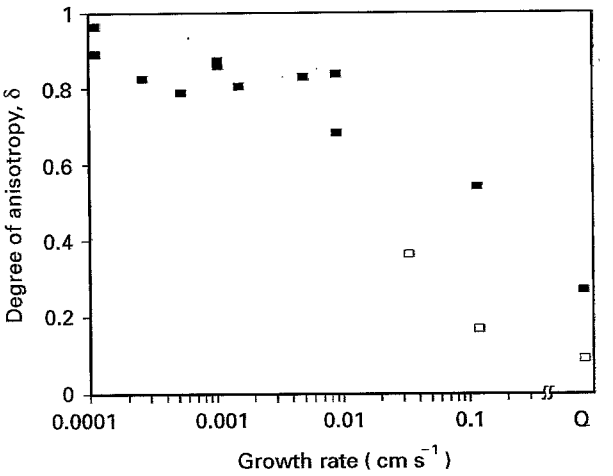

Figure 5 Variation of the degree of anisotropy, δ, with growth rate. (□) radial directionality.

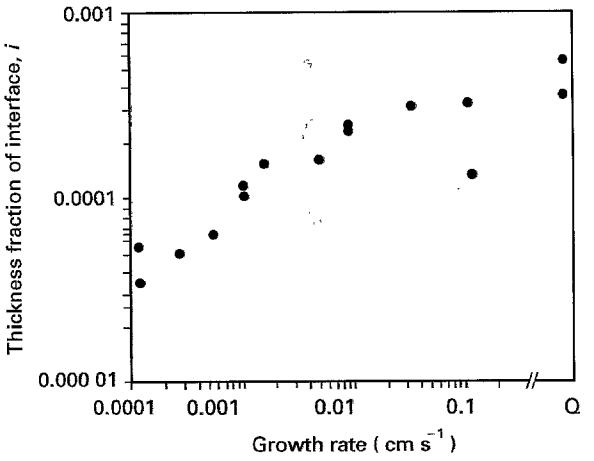

Figure 6 Variation of the thickness fraction of the interface phase with growth rate.

where $k = y/x$. The variation of δ with growth rate is given in Fig. 5. As expected, δ gradually decreases with growth rate, and especially at high growth rates it approaches zero, implying that the microstructure reveals a nearly isotropic nature. However, it is to be noted that the δ obtained at high growth rates does not accurately reflect the real microstructural anisotropy. As y decreases and x increases, the interface phase in front of the Sb block in the longitudinal direction of Fig. 4, which has been neglected in the present treatment, should be considered. As a result, at higher growth rates δ will have a somewhat lower value than it would have if the interface phase was taken into consideration. The data points, indicated by empty squares, in Fig. 5 represent δ associated with the radial directionality described above.

4.2. Contribution of interface phase to the electrical resistivity of the eutectic

As mentioned earlier, the higher measured value of $\rho\perp$ than that calculated from y and x (except for the specimen with 26 wt % In grown at 1.2×10^{-4} cm s^{-1}) is attributed to additional resistance due to the interface phase, and accordingly Equation 2 should be modified as follows to include the terms concerned with the interface phase (the equation is derived in the Appendix).

$$\frac{1}{\rho\perp} = \frac{1-xy}{\rho_{InSb}} + \frac{iy}{x\rho_i + (1-x)\rho_{InSb}} + \frac{xy}{x\rho_{Sb} + i\rho_i + (1-x)\rho_{InSb}} \quad (4)$$

where ρ_i is the resistivity of the interface phase and i is thickness fraction of the consolidated interface phase. i may be taken to be $2tx/d$, where t is the thickness of each interface and d is the diameter of each Sb rod. The interface is assumed to be a two atomic (In and Sb) layer with $t = 7 \times 10^{-8}$ cm. Rod diameter, for the convenience of calculation, the triangular rod morphology of the eutectic Sb was regarded as cylindrical, can be calculated from the relation $\lambda V_{Sb}^{1/2}$. i is plotted against the growth rate in Fig. 6, and gradually increases with increasing growth rate. Putting i and the measured $\rho\perp$ values into Equation 4 gives ρ_i values, as listed in Table I. ρ_i values obtained have approximately the same order of about 10^6–10^7 μΩ cm. Scatter of ρ_i values within an order of magnitude does not seem to be serious when it is remembered that the values are intricately connected with both $\rho\perp$ and $\rho\parallel$ values independently measured. With increasing growth rates, a somewhat lower value is obtained; this arises probably from the rough assumption that the morphology of Sb is preserved to be rod-like at any growth rate; at higher growth rates the Sb phase will show no longer an elongated rod morphology, but rather an irregular fibrous type, so that an even larger value of Sb diameter could be used for the estimation of i. For the fast grown specimens with 26 wt % In, evaluation of ρ_i values is impossible because the measured $\rho\perp$s have such low values for negative resistivity to be obtained.

It is generally known that the interface plays a role as an electron scattering boundary, causing resistance to current flow. Its role was recognized as a contributory factor to bring about a higher measured $\rho\perp$ value than the theoretically estimated one [14]. On the other hand, it was also reported that this is unlikely at room temperature because the electron mean free path is extremely short compared to the interphase spacing [4]. However, contact resistance at the interface between the constituents has been incorporated in computing the thermal conductivity of the composites with imperfect interfaces [15, 16]. According to Schoutens and Rig [6], a mismatch between the theoretical and experimental $\rho\perp$ values was regarded as due to two factors; modified electrical resistivities of the matrix resulting from periodic variations in the bulk cross-section and a disturbance in electron transport due to non-uniformity of the electrical field. At any rate, the effect due to the presence of a second phase and the resulting interface between the constituents manifest itself as an increase of the measured $\rho\perp$ value. In the present treatment the consolidated

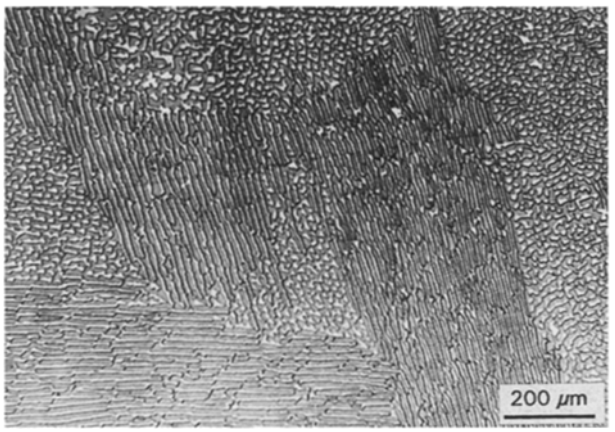

Figure 7 Micrograph showing a mixed structure comprising Sb plate and Sb rod (26 wt % In, $R = 1.2 \times 10^{-4}$ cm s^{-1}).

interface has been regarded as a third constituent bulk phase having a specific defect structure rather than a two-dimensional boundary which simply causes boundary scattering or a sudden change of the electrical field. The structure of the interface between the eutectic constituents has been interpreted as a network of dislocations [8, 17, 18], and also the interfacial energy was calculated from the dislocation model [8, 17]. In view of rough approximation in deriving Equations 1, 2 and 4, one need not give an absolute meaning to the numerical value of the interfacial resistivity, but its contribution should be appreciated.

The exceptions made for the specimen with 26 wt % In grown at 1.2×10^{-4} cm s^{-1} seems to arise from its unexpected microstructure, comprising both Sb plates and Sb rods, as revealed in Fig. 7. The uneven microstructure has been observed often, and interpreted in terms of structural rotation of the Sb phase [19]. The specimen would have a somewhat lower $\rho\perp$ if it is assumed that a fortuitous spatial arrangement of Sb plates is made in such a way as to allow favourable transverse conduction without exerting any negative effect on the longitudinal one.

5. Conclusions

The longitudinal and transverse resistivities measured in the unidirectionally solidified Sb–InSb eutectic alloy are higher than the calculated values based on the ideal assumption of complete alignment of Sb rods. Breaking of Sb rods leads to loss of microstructural anisotropy, resulting in the increase of $\rho\|$. Irrespective of the $\rho\perp$ value, the measured $\rho\|$ value therefore can be used to determine the degree of microstructural anisotropy. In contrast to $\rho\|$, $\rho\perp$ is strongly influenced by the presence of an interface phase between Sb and InSb. The mismatch between the measured and the calculated $\rho\perp$ value can also provide a clue for the evaluation of the resistivity of the interface phase.

Appendix

The composite resistor shown in Fig. 4 can be divided into four segments arranged parallel to each other. The resistance of each segmental resistor in transverse direction are

$$R_1 = \rho_{InSb}\frac{1}{(x+i)(i-y)}$$

$$R_2 = \rho_{Sb}\frac{x}{xy} + \rho_i\frac{i}{xy} + \rho_{InSb}\frac{1-x-i}{xy}$$

$$R_3 = \rho_i\frac{x+i}{iy} + \rho_{InSb}\frac{1-x-i}{iy}$$

$$R_4 = \rho_{InSb}\frac{1}{1-x-i}$$

With the assumption that $i \ll x$ and $i \ll y$, then

$$\frac{1}{\rho\perp} = \frac{1}{R\perp} = \frac{1}{R_1} + \frac{1}{R_2} + \frac{1}{R_3} + \frac{1}{R_4}$$

$$= \frac{1-xy}{\rho_{InSb}} + \frac{iy}{x\rho_i + (1-x)\rho_{InSb}} + \frac{xy}{x\rho_{Sb} + i\rho_i + (1-x)\rho_{InSb}}$$

References

1. M. H. MULAZIMOGLU, R. A. L. DREW and J. E. GRUZLESKI, *Metall. Trans.* **18A** (1987) 941.
2. *Idem, ibid.* **20A** (1989) 383.
3. I. H. MOON, I. S. AHN and Y. L. KIM, *J. Mater. Sci.* **16** (1981) 1367.
4. A. F. WHITEHOUSE, C. M. WARWICK and T. W. CLYNE, *ibid.* **26** (1991) 6176.
5. D. K. HALE, *ibid.* **11** (1976) 2105.
6. J. E. SCHOUTENS and F. S. ROIG, *ibid.* **22** (1987) 181.
7. F. S. ROIG and J. E. SCHOUTENS, *ibid.* **21** (1986) 2409.
8. W. K. LIEBMANN and E. A. MILLER, *J. Appl. Phys.* **34** (1963) 2653.
9. T. G. DIGGES, Jr. and R. N. TAUBER, *Metall. Trans.* **2** (1971) 1683.
10. M. J. SUK, G. H. CHOI, D. C. LEE and I. H. MOON, *Korean J. MRS* in press.
11. M. J. SUK and I. H. MOON, *J. Mater. Sci* **26** (1991) 4931.
12. G. T. MEADEN, "Electrical Resistance of Metals" (Plenum Press, New York, 1965) p. 147.
13. *Idem, ibid.* p. 15.
14. D. ABUKAY, K. V. RAO and S. ARAJS, *Fibre Sci. Technol.* **10** (1977) 313.
15. Y. BENVENISTE, *J. Appl. Phys.* **61** (1987) 451.
16. Y. BENVENSITE and T. MILOH, *Int. J. Engng Sci.* **24** (1986) 1537.
17. Y. UMEHARA and S. KODA, *Metallography* **20** (1987) 451.
18. A. GUHA, H. I. AARONSON and W. A. T. CLARK, *Metall. Trans.* **15A** (1984) 1623.
19. M. N. CROCKER, M. McPARLAN, D. BARAGAR and R. W. SMITH, *J. Cryst. Growth* **29** (1975) 85.

Received 15 December 1993
and accepted 22 June 1995